Carrier Lifetime Limitation of Industrial Ga-Doped Cz-Grown Silicon After Different Solar Cell Process Flows

Regina Post, Tim Niewelt, Wolfram Kwapil, and Martin C. Schubert

***Abstract*—Gallium-doped silicon material has been rapidly gaining importance in the photovoltaic industry as a boron-oxygen defect-free material with promising minority carrier lifetime. We investigate the influence of different cell process flows [passivated emitter and rear cell tunneling-oxide-passivating contact, and a "hot oxidation" process] on the bulk material quality of an industrial Ga-doped Cz-grown silicon material, as well as its light- and elevated temperature induced degradation degradation behavior under light at elevated temperature. We measure a generally high carrier lifetime level, which remains limited by an unknown recombination-active defect after most processes. Hydrogenation seems to passivate this unknown defect. In addition, we demonstrate that such high-quality p-type material can suffer noticeably by iron even for extremely low concentrations below 10^9 at/cm^3.**

***Index Terms*—Defect analysis, gallium doping, iron contamination, light- and elevated temperature induced degradation (LeTID), lifetime, silicon.**

I. Introduction

DESPITE progress of *n*-type silicon-based solar cell concepts, *p*-type silicon remains the dominant material in the photovoltaic (PV) industry [1]. Many processes and effects are well understood, the associated production is well established, and cell concepts based on p-type material, such as passivated emitter and rear cell (PERC), are widespread in industry. Until recently, the major share of the used *p*-type material has been boron-doped Czochralski-grown silicon (Cz-Si), despite it being prone to a significant degradation caused by the Boron-oxygen defect (BO defect) [2]. The light induced degradation (LID) caused by the BO defect is well-known [3] and mitigation strategies are developed and optimized [4], [5]. Another solution to the limitation imposed by the BO defect is to replace boron with a different *p*-type doping agent, for example gallium [2], [6]. It has been shown as early as 1999 that Ga-doped silicon allows for highly efficient solar cells resistant to LID [6], but commercial reasons hindered the introduction of Ga-doping into industry until recently. Now, Ga-doped Cz-Si is taking over the leading position as a doping agent rapidly. However, due to the limited experience with this type of silicon material, the question is raised how solar cell process steps affect the material quality and which limitations remain.

There are reports that Ga-doped silicon may be less prone to light- and elevated temperature induced degradation (LeTID) [7], although our recent work suggests that the LeTID behavior may be significant and is more complex [8]. It has been shown early on that Ga-doped material, even if reaching high carrier lifetimes, still stays well below the intrinsic limit [9], [10]. The reason for this shortcoming is not yet known. This article investigates the influence of different process routes on the silicon bulk quality and thus, highlights the potential of Ga-doped Cz-Si material for different cell technologies.

Manuscript received July 21, 2021; revised September 17, 2021; accepted September 21, 2021. Date of publication October 12, 2021; date of current version December 23, 2021. This work was supported in part by the German Federal Ministry for Economic Affairs and Energy and in part by the industry partners within the research cluster LIMES under Contract 0324204A and Contract 0324204C. (*Corresponding author: Regina Post.*)

Regina Post, Tim Niewelt, and Wolfram Kwapil are with the Fraunhofer Institute for Solar Energy Systems ISE, 79110 Freiburg, Germany, and also with the Institute for Sustainable Systems Engineering, University of Freiburg, 79110 Freiburg, Germany (e-mail: regina.post@ise.fraunhofer.de; tim.niewelt@ise.fraunhofer.de; wolfram.kwapil@ise.fraunhofer.de).

Martin C. Schubert is with the Faunhofer Institute for Solar Energy Systems ISE, 79110 Freiburg, Germany (e-mail: martin.schubert@ise.fraunhofer.de).

Color versions of one or more figures in this article are available at https://doi.org/10.1109/JPHOTOV.2021.3116017.

Digital Object Identifier 10.1109/JPHOTOV.2021.3116017

II. Sample Preparation and Characterization Procedure

A. Material and Processing

The investigated samples are high-quality industrial Ga-doped Cz-Si neighboring wafers obtained from a leading manufacturer, with a base resistivity of 0.9 Ωcm. The initial wafer thickness was 177±3 μm. To remove the damaged layer resulting from wafer sawing, 10 μm per side were etched off in a 40% potassium hydroxide solution. Then, the wafers were cleaned using HNF+SC1+SC2 solutions. After submission to variations of thermal treatments specified below, the sample surfaces were passivated on both sides to create four different symmetrical lifetime samples, that enable a comparison of different influences onto the bulk material. Fig. 1 shows a process overview. The sample set consists of the following.

One sample was directly passivated with an atomic layer deposition (ALD) Al_2O_3 layer of 10 nm at 180 °C in an Oxford OpAL system and activated with a 25 min forming gas anneal (FGA) at 450 °C. It is thus the sample closest to the as-grown state, having been subjected to the fewest external influences and the lowest temperature budget. This sample will be called "initial" in the following.

In contrast, the second sample was first subjected to an oxidation treatment at 1050 °C for 60 min and, after removal of

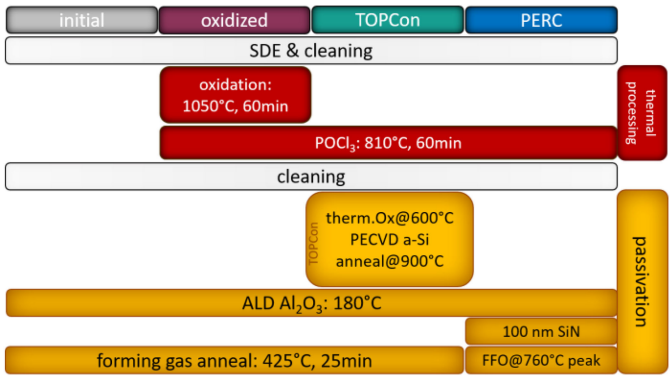

Fig. 1. Processing sequence for the four different samples.

the oxide layer, a $POCl_3$-diffusion at 810 °C for 60 min (with a subsequent etch-back of the phosphor silica glass (PSG) and the diffused region). This process sequence has been demonstrated to improve various monocrystalline silicon materials [11]–[13] and at the same time simulates the maximum thermal budget reasonable for solar cell processing. This sample was also passivated with an ALD Al_2O_3 layer at 180 °C and subsequent FGA. This sample will be called "oxidized" in the following.

The next two samples each represent a typical process route of two commonly used passivation schemes: PERC and tunneling-oxide-passivating contact (TOPcon). Both samples were first $POCl_3$-diffused and etched back, before receiving their individual passivation layers.

The sample called "PERC" received a 10 nm thick ALD Al_2O_3 layer deposited at 180 °C and a 100 nm thick SiN_x layer in a Roth&Rau MAiA PECVD deposition tool. It was subjected to a fast firing step at 760 °C peak temperature, activating the surface passivation. In cell processing this step also establishes the electrical contact with the metallization. The firing step is known to drive in hydrogen atoms from the SiN_x layer into the silicon bulk.

The sample called "TOPcon" was passivated with an n-TOPCon layer stack. It was shortly oxidized at 600 °C to obtain a thin SiO_x layer, then a P-doped a-SiC deposition was performed at 450 °C followed by a short anneal at 900 °C. Finally, an Al_2O_3 layer was deposited via ALD at 200 °C and an FGA at 450 °C was used to activate the TOPCon passivation. Although the *n*-type TOPCon layer is not optimized for p-type substrates, its passivation quality has been demonstrated to be excellent also on this doping type [12].

B. Measurement Techniques and Evaluation Procedures

For comparable lifetime data between the different samples we use steady-state photo luminescent (PL) images measured at various generation rates subsequently calibrated to carrier lifetime by modulated PL in the *modulum* tool to create spatially resolved, injection-dependent lifetime data sets [14]–[16]. To compare absolute lifetimes of different samples at a high lifetime level spatially resolved lifetime data should be used, to separate areas of undisturbed lifetime from areas with local inhomogeneities induced by wafer handling.

The samples were tested for iron contamination via two methods: PLI based Fe-imaging and an excess carrier density dependent lifetime investigation by means of quasi-steady-sate photo conductance (QSSPC). Fe-imaging can give a spatially resolved understanding of the iron contamination, while an excess carrier density dependent investigation is more sensitive and precise, as its evaluation is based on a large range of excess carrier density dependent lifetime.

The iron imaging was conducted via the *modulum* tool as described in [17] and [18]. To measure both recombination-active iron states (Fe_i/FeGa), the samples were first kept in the dark overnight to allow for the formation of FeGa pairs [18], [19]. A PL image was taken in this state, then the samples were illuminated with intense laser light (∼2.5 sun equivalents at 808 nm wavelength) to split the FeGa pairs and reach the Fe_i state, at which point another PL image is taken. The PL images in this procedure were taken at low generation rates and carefully chosen integration times to avoid changes in the Fe_i/FeGa system especially during the first PL image (in the FeGa state). Finally, a modulated PL lifetime measurement was conducted to calibrate the PL images to lifetimes images. The difference of these two lifetime images can be used to calculate an iron concentration map according to [17].

For a more precise iron evaluation the excess carrier density dependent lifetime of the samples in both states was measured with a Sinton Instruments lifetime tester [20]. After measuring the carrier lifetime in the FeGa state (after dark storage), the FeGa pairs were split by flashing the sample repeatedly in the lifetime tester, until no further change in the lifetime measurement was detected any more. Hence, the final lifetime measurement represents the highest achievable Fe_i fraction.

There are indications that the association of FeGa pairs is usually not complete in Ga-doped materials, although a saturation due to dark storage can be observed [18], [21], [22]. This means that the equilibrium of the FeGa/Fei system is not in a 100% FeGa state after dark storage. Hence evaluations under the assumption of 100% FeGa and 100% Fe_i state underestimate of the real iron content. In previous studies we have observed that the rearranged iron concentration may only constitute up to 40%–70% of the total iron concentration [18], [21], [22]. However, at this moment it is not possible to assess the exact share of rearranged iron with certainty and more research is necessary. Thus, it should be noted, that the iron concentration determined in the following likely only represents a lower limit [18], [21].

As demonstrated in a previous publication [8], the degradation extent during LeTID in Ga-doped samples is very sensitive to the excess carrier density. For example, it is possible to suppress LeTID, if the chosen excess carrier density is high enough. Hence, to test for LeTID the samples were subjected to an illumination of 0.1 sun equivalents (as opposed to 1 sun eq. usually used for LeTID testing in B doped samples [23]–[27]) and a temperature of 75 °C. Effective charge carrier lifetimes were repeatedly measured *ex situ* using a Sinton Instruments lifetime tester.

To assess further Shockley–Read–Hall (SRH) defects limiting the bulk lifetime the method of lifetime spectroscopy [28] was utilized. Assuming single-level defects, the SRH statistics is applied [29], [30], which calculates the defect-related recombination using the energy level of the defect within the bandgap E_t and the ratio k of the capture cross sections for

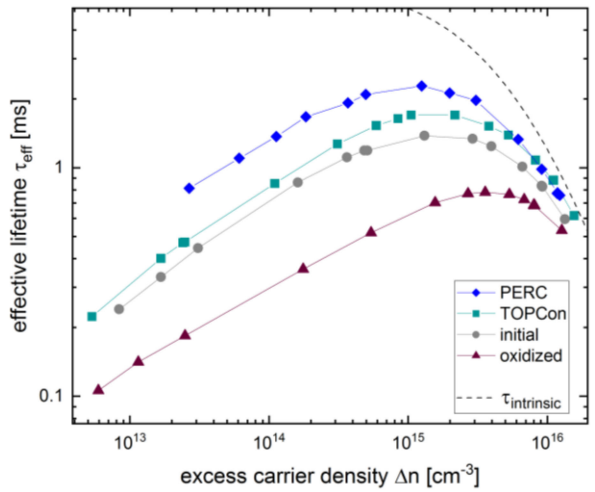

Fig. 2. Lifetime in the best regions of all samples at room temperature, measured via calibrated PL measurements in the Fe_i-state.

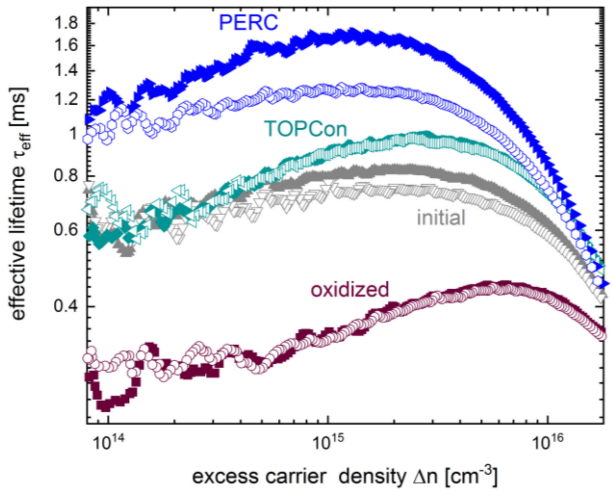

Fig. 3. Mean lifetime of all samples in FeGa state (open symbols) and Fe_i state (filled symbols). The lifetimes represent mean values averaging over the area of sensitivity of the QSSPC coil. The sample position in both states was kept unchanged.

electrons and holes. Since both parameters are specific for each defect, the combination of both can be used as a fingerprint for defect identification. Fitting SRH-statistics to a single excess carrier density dependent bulk lifetime measurement results in a continuum of E_t-k-pairs, that all describe the lifetime, thus the result is a solution surface [31]. In order to narrow down the solution surface to a single E_t-k-pair, a further variation of the measurement conditions beside the excess carrier density is necessary. This can be done by varying either the temperature (assuming temperature invariant k-values) or the doping. The intersect of all determined solution surfaces represents the defect parameters. In this article, we used the method of temperature variation, therefore the lifetime via calibrated PL images of the "TOPCon" sample was measured at six temperatures between 25 °C and 150 °C.

III. Results

A. General Influence of Cell Processing Steps on Ga-Doped Silicon

Fig. 2 displays the highest injection-dependent carrier lifetimes measured on each sample, which can be viewed as the upper lifetime limit (the potential) of the material after the given process sequence. To obtain this information, the region of the highest lifetime was selected for each sample and analyzed by lifetime-calibrated PL imaging. Hence, influences of scratches, wafer edges or [in case of the "oxidized" sample, see Fig. 4(a)] underlying defect formations were minimized.

The Ga-doped silicon of our study already has a very high lifetime above 1 ms (at $\Delta n \sim 10^{15}$ cm^{-3} for a base resistivity of 0.9 Ωcm) in the "initial" state, i.e., without additional (defect engineering) processes such as phosphorus gettering. As the results of the other process routes show, solar cell process steps can benefit or deteriorate the Ga-doped Cz silicon wafers. Although the oxidation and phosphorus gettering aimed at improving the lifetime [12], this process combination had the opposite effect on our samples. The PL images reveal [see Fig. 4(a)] that the oxidized sample shows a strong concentric structure, contrary to

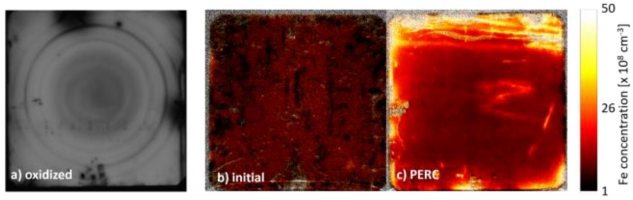

Fig. 4. Visual images of the samples. (a) PL image of the "oxidized" sample in arbitrary units. (b + c) images of the Fe concentration of (b) the "initial" sample and (c) the "PERC" sample. The calibration bar for both images is shown on the right.

the other samples. The ring-like structures suggest that the high-temperature oxidation activated or created defects that were not triggered by the processes applied to the other samples. The circular structure indicates that the defect is related to defects introduced during crystal growth and resembles typical patterns of silicon oxide precipitates [32]. Fortunately, oxide precipitates require prolonged anneals at sufficiently high temperatures to grow. The "TOPCon" process route, despite involving a 900 °C anneal to crystallize the a-SiC surface layer, results in slightly higher carrier lifetimes (up to 1.7 ms) than the "initial" sample. The latter can partially be attributed to the superior surface passivation [33]. The "PERC" process gives a significant boost to the carrier lifetime compared to the "TOPCon" processes, lifting it to values above 2 ms. This lifetime increase can be observed because in this experiment the surface saturation current J_0 of the "PERC" sample is comparable to the one determined for the "TOPCon" sample: $J_{0,\mathrm{TOPCon}} < 1$ fAcm^{-3}, $J_{0,\mathrm{PERC}} = 1.5$ fAcm^{-3} ($J_{0,\mathrm{initial}} = 2$ fAcm^{-3}) (all surface saturation currents are determined via a simultaneous fit of the bulk and surface limitation as described in [21] and [34]).

It should be mentioned that the lifetimes of all samples remain well below the intrinsic level (>4 ms) and a strong injection dependence of the lifetime is observed. Thus, it is likely that the material quality is affected by bulk defects, which are investigated in more detail in the next section.

B. Evaluation of the Iron Concentration

The strong injection dependence of the measured carrier lifetime suggests iron, a ubiquitous element, as a likely candidate for being the limiting defect. The iron content was analyzed using global QSSPC data and iron imaging [17].

Fig. 3 shows the lifetimes measured by photoconductance decay of all investigated samples after overnight dark storage (open symbols) and in saturated state after repeated flashing (filled symbols), while Fig. 4(b) and (c) display the lateral iron distribution for the "initial" and the "PERC" sample, respectively. Both methods indicate an iron contamination in the "initial" and "PERC" sample, whereas the "TOPCon" and the "oxidized" sample (Fe-imaging not shown) do not show a change in lifetime due to the illumination treatment.

The "initial" sample has not been subjected to high-temperature steps that could have caused significant Fe in-diffusion from unintentional surface contamination in the course of the processing. Therefore, the measurement indicates that the material itself contained a noticeable yet very low amount of iron in the as-grown state. The homogeneous iron distribution [see Fig. 4(b)] further supports the assumption of a material contamination. The determined iron concentrations, representing a lower limit, are: $[\mathrm{Fe}_{i,\mathrm{QSSPC}}] = 8 \times 10^8\ \mathrm{cm}^{-3}$ and $[\mathrm{Fe}_{\mathrm{i,\ imaging,\ average}}] = 6 \times 10^8\ \mathrm{cm}^{-3}$. Note that no $POCl_3$ diffusion had been performed on this sample. By contrast, the "TOPCon" sample, having been subjected to a phosphorus gettering, shows no Fe-induced lifetime instability, which implies that $POCl_3$ gettering is an effective countermeasure and supports the assumption that the "initial" sample was limited by grown-in iron. The "oxidized" sample has also undergone phosphorus gettering and does not show any Fe-related impact on the carrier lifetime. However, given the strong limitation due to other defects, the detection of iron is less sensitive and hence this sample cannot support or exclude this assumption.

Despite the $POCl_3$ diffusion, the "PERC" sample suffers from a noticeable iron contamination. The observed iron content is in the same range as the one determined for the "initial} sample, amounting to $[\mathrm{Fe}_{i,\mathrm{QSSPC}}] = 9 \times 10^8\ \mathrm{cm}^{-3}$. However, the iron contamination is not evenly distributed: As seen in Fig. 4(c), a higher concentration is found in curvy lines reminiscent of run-off traces. This pattern is typical for iron contamination picked up during wet chemical processing. The subsequent firing process, only present in the "PERC" process in our study, can facilitate in-diffusion of iron from the surfaces [35], [36]. However, note that the measured iron concentration is still very low, even if considering that the determined amount most likely is only a fraction of 40-70% of the real concentration.

C. Light- and Elevated Temperature-Induced Degradation

LeTID degradation is known to occur in all materials [23]–[27], with most existing literature dedicated to B-doped silicon. In numerous studies on this material type, a correlation of the LeTID degradation with hydrogenation has been demonstrated [37]–[40].

A similar dependence can be drawn from our results shown in Fig. 5. As expected from Fig. 3, the "initial," "TOPCon" and "PERC" sample start at a comparable lifetime level around 1 ms, while the "oxidized" sample initially has a lifetime of 0.3 ms. Due to the similar starting lifetimes of the former three samples,

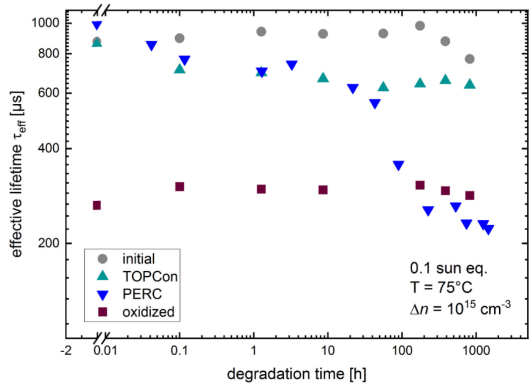

Fig. 5. Lifetime at an excess carrier density of $10^{15}\,\mathrm{cm}^{-3}$ during LeTID degradation under an illumination of 0.1 sun eq. and a temperature of $T = 75$ °C.

the excess carrier densities and thus the degradation conditions are comparable. The "PERC" sample is the only one showing a strong degradation under LeTID conditions. A slight dip may be observed in the "TOPCon" sample, whereas the 'initial' and 'oxidized' samples even seem to benefit slightly from the applied treatment.

Therefore, the ambiguous role of hydrogen in the silicon bulk is evident: On one hand, it leads to a significant increase in the carrier lifetime (comparing the "TOPCon" and the "PERC" samples before LeTID treatment, cf. Figs. 2 and 3 by passivating recombination-active defects. On the other hand, this improvement comes at the cost of increased susceptibility to LeTID. Please note that the full passivation potential of the TOPCon stack also requires hydrogen introduced into the sample [41]–[45]. This can be done in several ways, as discussed in detail in [46]; it seems that our choice in this article (deposition of Al_2O_3 layer together with FGA) also facilitates a certain extent of LeTID.

D. Evaluation of the Limitations

It has been observed in several publications that Ga-doped samples do not reach the intrinsic lifetime limit, e.g., [7], [9]. Some published lifetime data [7], [9] indicates a significant injection dependence, which is, in contrast, not supported in other publications [10]. The reason for these different behaviors and the observed limitations has not been identified yet. In this section, we attempt to break down the origin of the limitation for the investigated samples.

For the "oxidized" sample the injection dependence can be attributed to the additional defects triggered by the high-temperature steps [ring like structures in Fig. 4(a)], as they dominate the lifetime measurements. Given the circular structure observed in PL imaging [c.f. Fig. 4(a)] the limitation can likely be attributed to silicon oxide precipitation [32]. While the peak temperature of the applied oxidation process should suffice to dissolve preexisting precipitate nuclei, it is possible that this specific wafer held too large nuclei. It should be noted that we have observed similar pattern occurrence in other Cz Si materials subjected to the same thermal treatment. With our limited knowledge on the specific growth conditions of the used material we cannot evaluate further whether this may be a general issue of Ga-doped Cz Si.

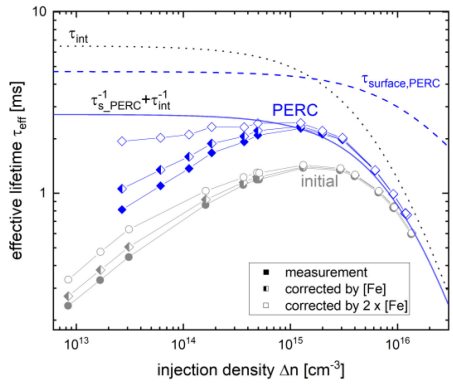

Fig. 6. Potential lifetimes of the "initial" sample and the "PERC" sample. The full symbols display the measured lifetimes of both samples in Fe_i-state. The half-filled symbols show a correction for the iron concentration determined via FeGa/Fe_i-splitting, while the hollow symbols show a correction for twice the amount, assuming that the splitting is not complete. The blue solid line further indicates the maximum lifetime of the "PERC" sample limited only by intrinsic and surface recombination.

As demonstrated, the "initial" and "PERC" sample are limited by iron contamination. This raises the question whether the injection dependence we observe can be attributed exclusively to iron. To this end, we corrected the lifetimes of the "initial" and the "PERC" sample by the recombination imposed by the measured iron concentration. Since the determined iron concentration likely only represents a fraction of the real iron content in the sample, we also corrected the lifetime for twice the determined amount (as we assume the dissociated share to be between 40%–70%) for comparison. The lifetimes determined by calibrated PL measurements (see Fig. 2) were used for correction, assuming they represent 100% Fe_i-state. Injection dependent curves for SRH lifetime limitations in Fe_i-state were calculated for the determined iron amount and twice that amount with the parameters suggested by Istratov *et al.* [47]. These SRH lifetime limitations were then used to correct the measured lifetimes.

The measured lifetime in Fe_i-state, as well as both corrections are displayed in Fig. 6. It is obvious that for the "initial" sample the injection dependence still remains, even after a correction for twice the determined iron amount (please note that corrections for even higher iron concentrations proved to be invalid, as they resulted in systematically distorted injection dependencies, showing jumps and unphysical trends). For the "PERC" sample, on the other hand, a correction by twice the determined iron concentration yields a lifetime with an almost flat injection dependence. Interestingly, the resulting lifetime curve is close to the maximum lifetime of this sample (blue solid line in Fig. 6), consisting of only intrinsic and surface recombination (with a determined value of $J_{0,\mathrm{PERC}} = 1.5$ fAcm^{-3}).

Therefore, we conclude that the "PERC" sample very likely is only limited by iron and surface recombination. In addition, this result can be seen as an indication for the systematic underestimation (by half) of dissolved iron in Ga-doped Cz-Si in the course of the standard exploitation of the Fe_i/FeGa metastability. Although not surprising, it is worth pointing out that even extremely low iron concentrations (< 2 x 10^9 cm^{-3}) can significantly limit samples with a high general lifetime level.

However, the Fe contamination alone cannot explain the lifetime limitation in the "initial" sample (see Fig. 6); further the "TOPCon" sample still shows an injection dependent lifetime despite being unaffected by iron and showing little impact of LeTID. An obvious difference between these two and the "PERC" samples is the amount of hydrogenation. The unknown, deleterious defect could possibly be passivated by hydrogen in the "PERC" sample, whereas it is still active in samples without significant introduction of hydrogen. This conclusion could possibly explain the different lifetime limitations observed in Ga-doped materials in the literature [7], [9], [10], as the only lifetime measurements without significant injection dependence by Lim *et al.* [10] also introduced hydrogen into the samples by firing.

We attempted a defect analysis via temperature and injection dependent defect spectroscopy using the "TOPCon" sample with the assumption of one single-level defect (note that the "initial" sample is not suitable for further analysis, as the observed iron limitation introduces significant uncertainties). However, the defect analysis (not shown) turned out to be inconclusive, as defect investigations on high lifetime samples are very challenging. The precise knowledge of the intrinsic recombination is of paramount importance in the analysis of high-lifetime samples. Although an improved parametrization for the intrinsic recombination is in development [48], which eliminates current insufficiencies at room temperature [12], detailed information on the temperature dependence of the Auger process—necessary for temperate and injection dependent lifetime spectroscopy (TIDLS)—is still lacking.

IV. Conclusion

We demonstrated that Ga-doped silicon has a high lifetime potential and thus is very well suited for solar cell fabrication. The investigated Ga-doped Cz Si material shows high carrier lifetimes already in its initial state, which can be further improved by typical PERC or TOPCon cell processing routes. On the other hand, high temperature treatments, such as oxidation may give rise to silicon oxide precipitation and should be applied with care. Further, we demonstrated that hydrogenation improves the lifetime even after a gettering step, probably passivating a yet unknown defect in Ga-doped samples. However, this improvement comes at the cost of making the sample susceptible to subsequent LeTID degradation. Therefore, a cell processing route should incorporate an optimized hydrogenation step which balances the tradeoff between beneficial and deleterious impacts. We also demonstrated that Ga-doped wafers of this high material quality are extremely sensitive to minute amounts of Fe, highlighting the importance of cleanest environments and tight process control during cell production. Finally, we observed that unhydrogenated Ga-doped samples suffer from a lifetime limitation likely linked to a bulk defect. Further work is needed to identify this defect.

References

[1] "International technology roadmap for photovoltaic (ITRPV): 2020 results," Int. Technol. Roadmap Photovolt., Frankfurt, Germany, 2021.
[2] K. Bothe and J. Schmidt, "Electronically activated boron-oxygen-related recombination centers in crystalline silicon," *J. Appl. Phys.*, vol. 99, no. 1, 2006, Art. no. 13701.

[3] T. Niewelt, S. Mägdefessel, and M. C. Schubert, "Fast in-situ photoluminescence analysis for a recombination parameterization of the fast BO defect component in silicon," *J. Appl. Phys.*, vol. 120, no. 8, 2016, Art. no. 85705.

[4] A. Herguth and G. Hahn, "Kinetics of the boron-oxygen related defect in theory and experiment," *J. Appl. Phys.*, vol. 108, no. 11, 2010, Art. no. 10.

[5] B. Hallam *et al.*, "Eliminating light-induced degradation in commercial p-type Czochralski silicon solar cells," *Appl. Sci.*, vol. 8, no. 1, 2018.

[6] S. W. Glunz, S. Rein, J. Knobloch, W. Wettling, and T. Abe, "Comparison of boron- and gallium-doped p-type Czochralski silicon for photovoltaic application," *Prog. Photovolt: Res. Appl.*, vol. 7, no. 6, pp. 463–469, 1999.

[7] N. E. Grant, J. R. Scowcroft, A. I. Pointon, M. Al-Amin, P. P. Altermatt, and J. D. Murphy, "Lifetime instabilities in gallium doped monocrystalline PERC silicon solar cells," *Sol. Energy Mater. Sol. Cells*, vol. 206, 2020, Art. no. 110299.

[8] W. Kwapil, J. Dalke, R. Post, and T. Niewelt, "Influence of dopant elements on degradation phenomena in B- and Ga-doped Czochralski-grown silicon," *Sol. RRL*, vol. 5, no. 5, pp. 1–10, 2021.

[9] A. Metz, T. Abe, and R. Hezel, "Gallium-doped Czochralski grown silicon: A novel promising material for the PV-industry," in *Proc. 16th Eur. Photovolt. Solar Energy Conf. Exhib.,* 2000.

[10] B. Lim, A. Merkle, R. Peibst, T. Dullweber, Y. Wang, and R. Zhou, "LID-free PERC+ solar cells with stable efficiencies up to 22.1%, 2200," in *Proc. 35th Eur. Photovolt. Solar Energy Conf. Exhib.*, 2018, pp. 359–365.

[11] B. A. Veith-Wolf, S. Schäfer, R. Brendel, and J. Schmidt, "Reassessment of intrinsic lifetime limit in n-type crystalline silicon and implication on maximum solar cell efficiency," *Sol. Energy Mater. Sol. Cells*, vol. 186, pp. 194–199, 2018.

[12] T. Niewelt *et al.*, "Taking monocrystalline silicon to the ultimate lifetime limit," *Sol. Energy Mater. Sol. Cells*, vol. 185, pp. 252–259, 2018.

[13] N. E. Grant *et al.*, "Superacid-treated silicon surfaces: Extending the limit of carrier lifetime for photovoltaic applications," *IEEE J. Photovolt.*, vol. 7, no. 6, pp. 1574–1583, Nov. 2017.

[14] J. A. Giesecke, B. Michl, F. Schindler, M. C. Schubert, and W. Warta, "Minority carrier lifetime of silicon solar cells from quasi-steady-state photoluminescence," *Sol. Energy Mater. Sol. Cells*, vol. 95, no. 7, pp. 1979–1982, 2011.

[15] T. Trupke, R. A. Bardos, and M. D. Abbott, "Self-consistent calibration of photoluminescence and photoconductance lifetime measurements," *Appl. Phys. Lett.*, vol. 87, no. 18, 2005, Art. no. 184102.

[16] H. Höffler *et al.*, "Review and recent development in combining photoluminescence- and electroluminescence-imaging with carrier liftime measurements via modulated phtoluminescence at variable temperatures," in *37th EU PVSEC. Proc. Photovolt. Solar Energy Conf. Exhib.*, 2020, pp. 264–276.

[17] D. Macdonald, J. Tan, and T. Trupke, "Imaging interstitial iron concentrations in boron-doped crystalline silicon using photoluminescence," *J. Appl. Phys.*, vol. 103, no. 7, 2008, Art. no. 73710.

[18] R. Post, T. Niewelt, J. Schön, F. Schindler, and M. C. Schubert, "Imaging interstitial iron concentrations in gallium-doped silicon wafers," *Phys. Status Solidi (A)*, vol. 121, 2019, Art. no. 1800655.

[19] D. Macdonald, T. Roth, P. N. K. Deenapanray, K. Bothe, P. Pohl, and J. Schmidt, "Formation rates of iron-acceptor pairs in crystalline silicon," *J. Appl. Phys.*, vol. 98, no. 8, 2005, Art. no. 83509.

[20] R. A. Sinton and A. Cuevas, "Contactless determination of current–voltage characteristics and minority-carrier lifetimes in semiconductors from quasi-steady-state photoconductance data," *Appl. Phys. Lett.*, vol. 69, no. 17, pp. 2510–2512, 1996.

[21] R. Post, "Assessment of defect characterization via lifetime spectroscopy," Ph.D. thesis, Dept. Phys., Univ. Constance, Konstanz, Germany, 2021.

[22] P. Palinginis *et al.*, "Photovoltaics international: Pioneering the industrialization of PERC technology: A review of the development of mono- and bifacial PERC solar cells at solarworld," *Photovolt. Int., Sol. Media Ltd.,* vol. 42, pp. 49–72, 2019.

[23] K. Ramspeck *et al.*, "Light induced degradation of rear passivated mc-Si solar cells," in *Proc. 27th Eur. Photovolt. Solar Energy Conf. Exhib.*, 2012, pp. 861–865.

[24] F. Kersten *et al.*, "Degradation of multicrystalline silicon solar cells and modules after illumination at elevated temperature," *Sol. Energy Mater. Sol. Cells*, vol. 142, pp. 83–86, 2015.

[25] T. Niewelt, F. Schindler, W. Kwapil, R. Eberle, J. Schön, and M. C. Schubert, "Understanding the light-induced degradation at elevated temperatures: Similarities between multicrystalline and floatzone p-Type silicon," in *Proc. 33rd Eur. Photovolt. Solar Energy Conf. Exhib.*, 2017, Art. no. 13701.

[26] D. Chen *et al.*, "Evidence of an identical firing-activated carrier-induced defect in monocrystalline and multicrystalline silicon," *Sol. Energy Mater. Sol. Cells*, vol. 172, pp. 293–300, 2017.

[27] H. C. Sio *et al.*, "Light and elevated temperature induced degradation in p-type and n-type cast-grown multicrystalline and mono-like silicon," *Sol. Energy Mater. Sol. Cells*, vol. 182, pp. 98–104, 2018.

[28] S. Rein, T. Rehrl, W. Warta, and S. W. Glunz, "Lifetime spectroscopy for defect characterization: Systematic analysis of the possibilities and restrictions," *J. Appl. Phys.*, vol. 91, no. 4, pp. 2059–2070, 2002.

[29] W. Shockley and W. Read, "Statistics of the recombinations of holes and electrons," *Phys. Rev.*, vol. 87, no. 5, pp. 835–842, 1952.

[30] R. Hall, "Electron-hole recombination in germanium," *Phys. Rev.*, vol. 87, no. 2, 1952, Art. no. 387.

[31] S. Rein, *Lifetime Spectroscopy: A Method of Defect Characterization in Silicon for Photovoltaic Applications,* 1st ed. Berlin, Germany: Springer, 2005, pp. 69–257.

[32] J. Haunschild, I. Reis, J. Geilker, and S. Rein, "Detecting efficiency-limiting defects in Czochralski-grown silicon wafers in solar cell production using photoluminescence imaging," *Phys. Status Solidi RRL*, vol. 5, no. 5/6, pp. 199–201, 2011.

[33] B. Steinhauser, J.-I. Polzin, F. Feldmann, M. Hermle, and S. W. Glunz, "Excellent surface passivation quality on crystalline silicon using industrial-scale direct-plasma TOPCon deposition technology," *Sol. RRL*, vol. 2, no. 7, 2018, Art. no. 1800068.

[34] B. Hammann and R. Post, "On the surface passivation for material characterization of silicon," 2021.

[35] J. Schön, M. C. Schubert, W. Warta, H. Savin, and A. Haarahiltunen, "Analysis of simultaneous boron and phosphorus diffusion gettering in silicon," *Phys. Statist. Sol. (A)*, vol. 207, no. 11, pp. 2589–2592, 2010.

[36] D. Macdonald, A. Cheung, and A. Cuevas, "Gettering and poisoning of silicon wafers by phosphorus diffused layers," in *Proc. 3rd World Conf. Photovolt. Energy Convers.*, 2003, pp. 1336–1339.

[37] T. Niewelt, F. Schindler, W. Kwapil, R. Eberle, J. Schön, and M. C. Schubert, "Understanding the light-induced degradation at elevated temperatures: Similarities between multicrystalline and floatzone p-type silicon," *Prog. Photovolt. Res. Appl.*, vol. 99, 2017, Art. no. 13701. [Online]. Available: http://onlinelibrary.wiley.com/store/10.1002/pip.2954/asset/pip2954.pdf?v=1&t=jcg0hqdk&s=b5d5af99f4ebef846bb85803fd3d3c12eb1b2fa0

[38] D. Chen *et al.*, "Hydrogen-induced degradation: Explaining the mechanism behind light- and elevated temperature-induced degradation in n- and p-type silicon," *Sol. Energy Mater. Sol. Cells*, vol. 207, 2020, Art. no. 110353.

[39] T. H. Fung *et al.*, "Influence of bound hydrogen states on carrier-induced degradation in multi-crystalline silicon," *AIP Conf. Proc.*, vol. 1999, 2018, Art. no. 130004.

[40] D. Bredemeier, D. C. Walter, R. Heller, and J. Schmidt, "Impact of hydrogen-rich silicon nitride material properties on light-induced lifetime degradation in multicrystalline silicon," *Phys. Status Solidi RRL*, vol. 13, no. 8, 2019, Art. no. 1900201.

[41] F. Feldmann, M. Simon, M. Bivour, C. Reichel, M. Hermle, and S. W. Glunz, "Efficient carrier-selective p- and n-contacts for si solar cells," *Sol. Energy Mater. Sol. Cells*, vol. 131, pp. 100–104, 2014. [Online]. Available: http://www.sciencedirect.com/science/article/pii/S092702481400289X

[42] T. N. Truong *et al.*, "Hydrogenation mechanisms of poly-Si/SiO_x Passivating contacts by different capping layers," *Sol. RRL*, vol. 4, no. 3, 2020, Art. no. 1900476.

[43] T. N. Truong *et al.*, "Hydrogenation of phosphorus-doped polycrystalline silicon films for passivating contact solar cells," *ACS Appl Mater Interfaces*, vol. 11, no. 5, pp. 5554–5560, 2019.

[44] B. W. van de Loo *et al.*, "On the hydrogenation of poly-Si passivating contacts by Al_2O_3 and SiN thin films," *Sol. Energy Mater. Sol. Cells*, vol. 215, 2020, Art. no. 110592.

[45] M. Schnabel *et al.*, "Hydrogen passivation of poly-Si/SiO_x contacts for Si solar cells using Al_2O_3 studied with deuterium," *Appl. Phys. Lett.*, vol. 112, no. 20, 2018, Art. no. 203901.

[46] J.-I. Polzin, B. Hammann, T. Niewelt, W. Kwapil, M. Hermle, and F. Feldmann, "Thermal activation of hydrogen for defect passivation in poly-Si based passivating contacts," *Sol. Energy Mater. Sol. Cells*, vol. 230, 2021, Art. no. 111267.

[47] A. A. Istratov, H. Hieslmair, and E. R. Weber, "Iron and its complexes in silicon," *Appl. Phys. A*, vol. 69, no. 1, pp. 13–44, 1999.

[48] T. Niewelt *et al.*, "Reassessment of the intrinsic bulk recombination in crystalline silicon," 2021.